Research Square

Preprints are preliminary reports that have not undergone peer review.
They should not be considered conclusive, used to inform clinical practice,
or referenced by the media as validated information.

Freespace twistronics for optical supertopologies

Yijie Shen

yijie.shen@ntu.edu.sg

Nanyang Technological University https://orcid.org/0000-0002-6700-9902

Vasu Dev

Nanyang Technological University

Article

Keywords:

Posted Date: January 13th, 2026

DOI: https://doi.org/10.21203/rs.3.rs-8188826/v1

License: This work is licensed under a Creative Commons Attribution 4.0 International License.
Read Full License

Additional Declarations: There is **NO** Competing Interest.

Version of Record: A version of this preprint was published at Light: Science & Applications on November 6th, 2026. See the published version at https://doi.org/10.1038/s41377-026-02533-w.

Freespace twistronics for optical supertopologies

Vasu Dev[1] and Yijie Shen[1,2,*]

[1] *Centre for Disruptive Photonic Technologies, School of Physical and Mathematical Sciences, Nanyang Technological University, Singapore 637371, Republic of Singapore*
[2] *School of Electrical and Electronic Engineering, Nanyang Technological University, Singapore 639798, Singapore*

(Dated: November 24, 2025)

Twistronics, the study of moiré superlattices of twisted bilayer 2D materials creating nontrivial physical effects, has recently revolutionized diverse subjects from materials to optoelectronics, nanophotonics, and beyond. Here, breaking the reliance on materials, we present twistronics in higher-dimensional free space, where the twisted lattice is not a layer of 2D material but a 3D propagating light field with topological textures. Moiré structured light with a twist angle can generate a rich set of high-dimensional topologies, including skyrmionium bags, skyrmion bag superlattices, skyrmion clusters, and quasicrystals, with controllable symmetry. Many of these textures have not been reported before. Importantly, in contrast to prior moiré superlattices, our freespace moiré textures maintain their topologies over long propagation distances, showing nondiffractive behavior and robustness against perturbations and obstacles. Our work unlocks higher dimensions to manipulate moiré photonics with high-capacity topologies to address the challenges of robust information transfer and encryption.

Twistronics – the study of the evolution of physical properties in two-dimensional materials induced by a controlled twist between adjacent layers. The interference of two periodic lattices with a relative twist induces a moiré pattern, which has transited from everyday textiles to the scientific frontier[1]. Remarkably, the moiré superlattice patterns on the twisted two atomically thin layers can generate entirely novel physical properties with "$1+1 \gg 2$" scheme, e.g., the superconductivity[2,3], correlated insulator behaviour[4], tunable spin-polarized phases[5], flat-band and quantum geometry[6] in twisted bilayer and multilayer graphenes. Moreover, twistronics has been applied to a variety of advanced materials, where specific twist angles known as 'magic' angles can radically alter the electronic and photonic properties of materials[7]. For instance, the excitonic devices with twisted van der Waals heterostructures[8], photonic hyperbolic polaritons excited on twisted α-MoO_3[9], optical Hall effect enabled by spiral multilayer WS_2[10]. Twisted photonic crystals can be used to localize light fields[11] and enhance reconfigurable and singular nanolasers[12,13]. Recently, twistronics was extended to hydrodynamics to control energy localization in fluid[14], and also to surface plasmon plariton to create nontrivial topological textures of evanescent waves on metal surface[15].

However, the existing concept of twistronics relies on material platforms, where the related physical phenomena occur primarily at low-dimensional surfaces. Furthermore, the resulting moiré phenomena are typically confined to near-field interactions or surface-bound excitations, leaving their extension into freely propagating wave systems largely unexplored. These constraints highlight the need for a framework that can realize moiré physics and topological interactions in higher-dimensional, reconfigurable physical systems.

The investigation of novel topological quasiparticles, including and beyond skyrmions, has become a central pursuit in modern physics aimed at achieving robust and reconfigurable information carriers. Recent advances have revealed a wide range of such excitations across diverse physical systems, including antiferromagnetic merons[16], magnetic skyrmion bundles[17], hopfions[18], torons in liquid crystals[19], optical spin textures[20], optical skyrmion and meron lattices[21–26], hopfion crystals[27], and other complex topologies observed in both light and matter systems[28,29].

Here we extend the principles of twistronics into the emerging domain of topological light waves, where structured light fields carry topological quasiparticle textures and propagate in free space[30]. Freespace twistronics provides a unified framework for generating a broad family of optical *supertopologies*. These supertopologies include skyrmionium bags, skyrmion bags, skyrmion clusters, meron-antimeron cluster and topological quasicrystals that propagate nondiffractively and remain stable against perturbations, representing a new class of topological light states beyond conventional material systems.

Important features of the supertopologies: (1) Supertopologies are generated by twisting two volumes of topological optical lattices, giving rise to complex moiré interference fields with novel topologies. The same framework can also reproduce recently discovered configurations such as topological quasicrystals[31–33] and skyrmion bags[15] in plasmonic systems. (2) These supertopologies propagate in free space over extended distances without diffraction, maintaining both their geometric scale and topological structure. (3) Supertopologies are intrinsically resilient to strong perturbations and exhibit self-healing in topology upon partial obstruction. Therefore, our results establish freespace twistronics as a foundational platform for investigating and engineering topological properties of light.

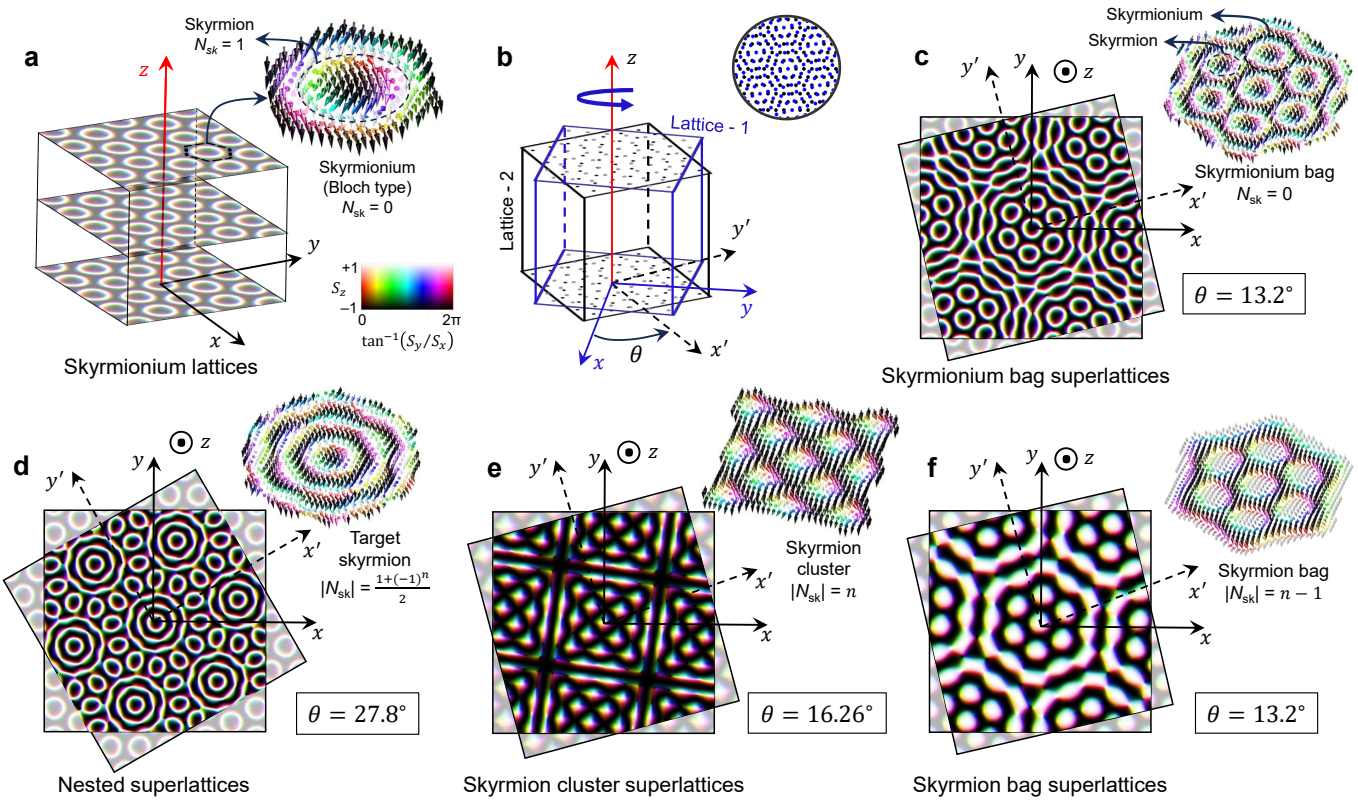

FIG. 1: **Concept of freespace twistronics and supertopologies.** (a) A basic freespace topological optical lattice field, which hosts C_6 symmetric skyrmionium lattices at each x-y plane and propagate along z-axis with nondiffraction. The inset highlights the skyrmionium texture as an unit cell at a transverse plane, where the inner skyrmion with unit topology is marked by dashed line. (b) Schematic of the morié pattern formed by superimposing two topological optical lattice fields (blue and black, where the dots represent centers of unit cells) with a twisted angle θ to z-axis. The inset shows a schematic morié superlattice pattern at a transverse plane. (c) The resultant morié structured light shows skyrmionium bag superlattices when $\theta = 13.2°$. The inset shows a skyrmionium bag, where multiple elementary skyrmioniums are surrounded by a bag skyrmioniums. (d) Nested superlattices with target-skyrmion-skyrmionium mixed topology obtained when $\theta = 27.8°$. The inset highlights a target skyrmion composed by multiple radially nested skyrmions with number of $n > 2$. (e) Skyrmion cluster superlattices in twisted bi-volume C_4 skyrmion lattices when $\theta = 16.26°$. The inset shows a skyrmion cluster texture composed by n skyrmions with total skyrmion number of $|N_{\rm sk}| = n$. (f) Skyrmion bag superlattices in twisted bi-volume C_6 skyrmion lattices, when $\theta = 13.2°$. The insert shows a skyrmion bag with n elementary skyrmions surrounded by a bag skyrmion with total skyrmion number of $|N_{\rm sk}| = n - 1$.

I. FREESPACE TWISTRONICS

Freespace twistronics establishes high-dimensional topological optical lattices as a new platform for moiré engineering, transcending the limits of two-dimensional materials and plasmonic media. In contrast to conventional twistronics, where moiré effects arise from electronic coupling between stacked layers, the optical version relies purely on field superposition and is therefore free from material constraints. This freedom enables access to higher-dimensional and dynamically reconfigurable moiré geometries that are challenging to realize in condensed matter systems.

We first develop a method to generate topological optical lattices with high phase stability and accuracy, and then apply freespace twistronics to obtain nontrivial high-dimensional topologies. The lattices are generated through the principle of N-wave interference, in which two structured light fields with binary and helical phase distributions and orthogonal polarizations are superimposed. In the Fourier domain, such lattices can be expressed as an array of N discrete point sources, which is experimentally challenging to realize. Therefore, to simplify, we approximate intensity of each point source with a Gaussian distribution. Therefore, the topological lattice in the Fourier domain can be expressed as:

$$\widetilde{U} = \sum_{j=1}^{N} \left[e^{-\frac{(x-\alpha_j)^2+(y-\beta_j)^2}{\omega_0^2}} \hat{\mathbf{e}}_{\mathbf{r}} + \mu e^{i(\theta_0+\phi_j)} e^{-\frac{(x-\alpha_j)^2+(y-\beta_j)^2}{\omega_0^2}} \hat{\mathbf{e}}_{\mathbf{l}} \right] \tag{1}$$

Where $\mu = A_2/A_1$ and A_1 and A_2 denote the am-

plitudes of the right- and left-circularly polarized (LCP and RCP) light fields, $\hat{\mathbf{e}}_\mathbf{r}$ and $\hat{\mathbf{e}}_\mathbf{l}$, respectively. The coordinates of the j-th Gaussian beamlet are given by $(\alpha_j, \beta_j) = \gamma(\cos\delta_j, \sin\delta_j)$, where $\gamma = d/\sqrt{1-\cos(2\pi/N)}$ and $\delta_j = \pi(2j-1)/N$ with $j = 1, 2, \ldots, N$. The parameter d represents the centre-to-centre separation between neighbouring Gaussian beamlets with the same beam waist ω_0. The discrete helical phase of each beamlet in LCP field is defined as $\phi_j = m[2\pi(j-1)/N]$, where m is the topological charge, and θ_0 is the global phase difference between the RCP and LCP. Following this formulation, we generate topological optical lattices exhibiting three characteristic symmetries: hexagonal C_6 skyrmionium lattices ($N = 6$), square C_4 skyrmion lattices ($N = 4$), and triangular C_3 meron–antimeron lattices ($N = 3$) (see the Extended Data Fig. 1).

Twisting two such topological lattices with a controlled relative angle gives rise to a freespace moiré field, where the superposition of the individual textures produces entirely new optical structures with novel topologies. The twist couples the intrinsic symmetry of each lattice to an additional spatial degree of freedom, leading to the formation of moiré superlattices with modified periodicity and symmetry. By varying the twist angle and the symmetry of the constituent lattices, we can engineer a broad range of high dimensional topological configurations that do not exist in the individual lattices. This tunability forms the basis of freespace twistronics, allowing direct optical access to moiré physics and emergent topology without the need for material interfaces. As the twist angle increases, the resultant field evolves from regular lattice geometry to complex quasiperiodic and clustered geometries. This continuous transformation marks the onset of high dimensional topological organization in free space, as shown in Fig. 1. For instance, a C_6 skyrmionium lattice beam is shown in Fig. 1(a), where the polarization Stokes vectors form a periodic array of skyrmioniums with sixfold rotational symmetry. Each unit cell is a hexagonal skyrmionium composed of two radially nested skyrmions with opposite polarity, giving a total skyrmion number of $N_{\mathrm{sk}} = 0$ (see inset). These topological lattices propagate along the z axis without diffraction, maintaining both their geometric size and topological structure. However, during the propagation, the phase rotation of the vortex lattice induces a gradual rotation of the helicity in each skyrmionium unit cell. Notably, in contrast to prior plasmonic topological lattices of Néel-type skyrmions[21,22], our freespace topological optical lattices offer additional degrees of freedom for controlling the skyrmion helicity. This allows the realisation of Bloch-type skyrmions and antiskyrmion lattices, as shown in Extended Data Fig. 2. Furthermore, by superimposing two volumes of such topological optical lattice fields, we generate moiré-structured light fields that host even more complex topologies, as shown in Fig. 1(b). By varying the twist angle, the lattice topology, and the underlying symmetry, a broad family of nontrivial moiré patterns can be realised.

Depending on the twist angle, the resulting moiré field can form either commensurate (periodic) or incommensurate (aperiodic) geometries. The incommensurate patterns lack translational symmetry, however, the rotational symmetry is preserved. Commensurate patterns are formed when lattice points from the both constituent topological lattices coincide, resulting in well-defined periodicity. The commensurability condition can be expressed as[15]

$$p\,\mathbf{a}_1 + q\,\mathbf{a}_2 \rightarrow q\,\mathbf{a}_1 + p\,\mathbf{a}_2, \tag{2}$$

where p and q are integers that define the coincidence between the primitive lattice vectors $\mathbf{a}_1$ and $\mathbf{a}_2$ of the two individual topological lattices.

In the commensurate regime, distinct topological superlattices are formed at specific twist angles. For instance, at $\theta = 13.2°$ the transverse field forms an optical superlattice composed of repeated supercells of complex skyrmionium bags — a topology not previously reported in any physical system (Fig. 1(c)). Each skyrmionium bag consists of multiple elementary skyrmionium cluster (e.g. $n = 7$) surrounded by a larger bag skyrmionium of opposite polarity. The outer bag skyrmionium offers an additional layer of topological protection for the embedded baby skyrmioniums. The central skyrmionium bag remains stable over a finite range of twist angles around $\theta = 13.2°$, beyond which the long-range periodic order gradually disappears, while a single central skyrmionium bag is preserved (see extended data Fig E3).

Controlled variation in the twist angle leads to a variety of new supertopologies, including optical nested superlattices. Figure 1(d) shows a twisted bi-volume C_6 skyrmionium lattice field at $\theta = 27.8°$, where a nondiffracting topological nested superlattice is formed in free space, where the skyrmioniums at the periphery are shared with neighboring super unit cells. Our freespace optical nested superlattice show a new class of higher-order mixed topology, where the centre hosts a target skyrmion composed of multiple radially nested skyrmions ($n > 2$) with a total skyrmion number $|N_{\mathrm{sk}}| = [1+(-1)^n]/2$, surrounded by a set of skyrmioniums. Furthermore, for specific twist angle, freespace twistronics leads to quasicrystaline geometry similar to those recently reported in plasmonic systems[31–33]. Quasicrystals are ordered but non-periodic systems that exhibit rotational symmetry while lacking translational symmetry, yet can host nontrivial topological textures such as the skyrmion–meron mixed states observed in plasmonic quasicrystals[32]. For $\theta = 30°$ freespace twistronics show a new class of higher-order mixed topology and can be termed as *supertopological quasicrystals*.

Furthermore, the individual C_6 skyrmionium lattices can be replaced with other topological lattices to obtain more diverse topologies. For instance, when C_4 skyrmion lattices are twisted, the moiré field at $\theta = 16.26°$ exhibits a new type of topology not previously reported — the skyrmion cluster superlattice (Fig. 1(e)). The inset shows a skyrmion-cluster supercell that hosts n

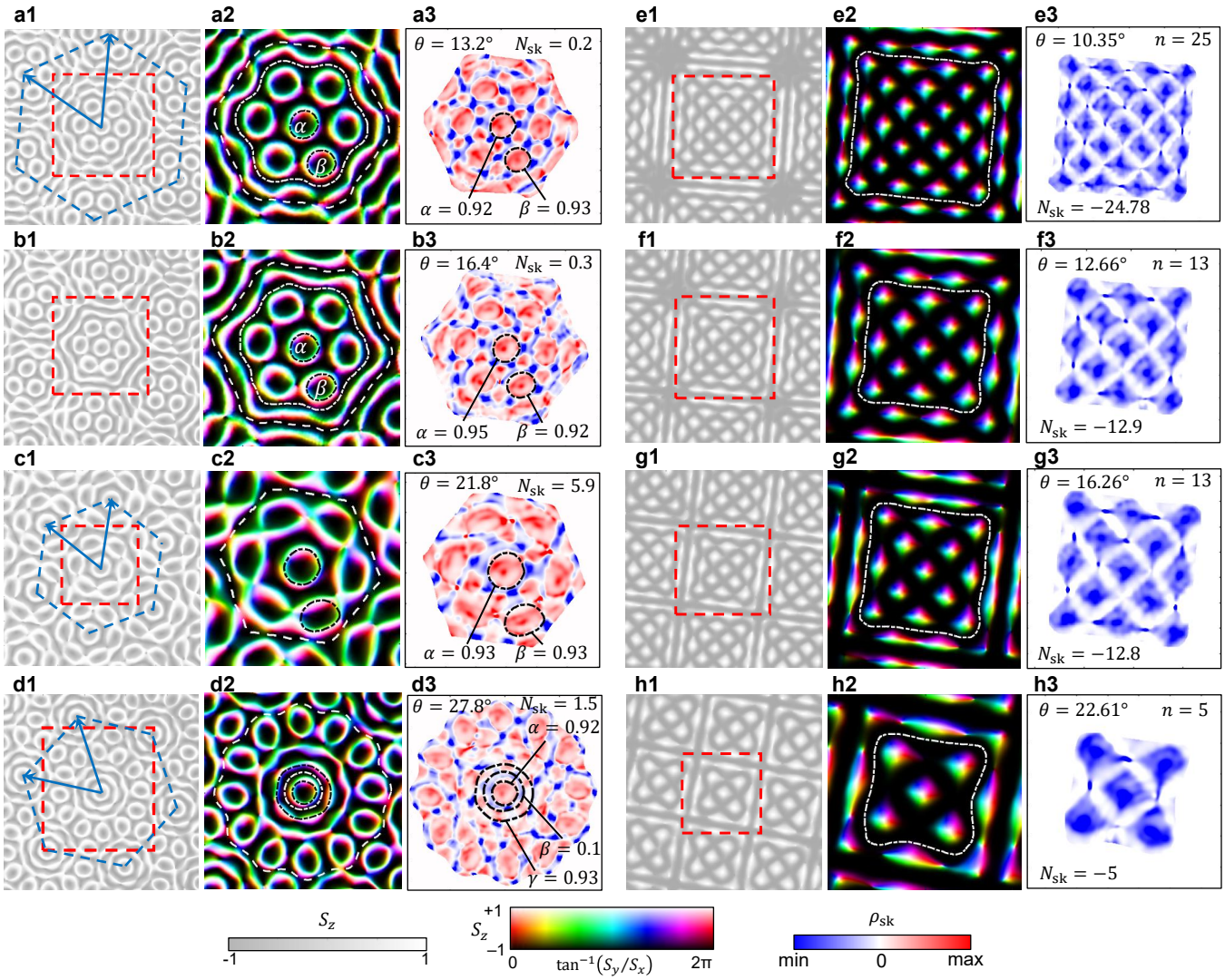

FIG. 2: **Experimental results of optical supertopologies.** Long-range distributions of S_z, spin textures of featured topological structures (in red-dashed line boxes of long-range patterns correspondingly), and corresponding skyrmion density distributions for twisted C_6 skyrmionium lattices obtaining (a1-a3) skyrmionium bag superlattices at $\theta = 13.2°$ (blue arrows mark the long-range periodic unit vectors of supercell), (b1-b3) isolated skyrmionium bag at $\theta = 16.4°$, (c1-c3) skyrmion cluster superlattices at $\theta = 21.8°$, (d1-d3) nested superlattice at $\theta = 27.8°$; and for twisted C_4 skyrmion lattices obtaining skyrmion cluster superlattices for different baby skyrmion numbers in supercell of (e1-e3) $n = 25$ at $\theta = 10.35°$, (f1-f3) $n = 13$ at $\theta = 12.66°$, (g1-g3) $n = 13$ at $\theta = 16.26°$, (h1-h3) $n = 5$ at $\theta = 22.61°$. The experimental skyrmion numbers N_{sk} of featured supertopologies, marked by big dashed lines in (a2-h2), are shown in (a3-h3), respectively. The experimental N_{sk} values of selected protected baby skyrmions ("α","β","γ",) marked by black dashed lines are shown in (a3-d3), correspondingly.

skyrmions of identical topology with a total skyrmion number of $|N_{sk}| = n$. Similarly, for C_6 skyrmion lattices, the moiré field at $\theta = 13.2°$ forms skyrmion bag superlattices (Fig. 1(f)). In a skyrmion bag, multiple elementary skyrmions ($n = 7$) are enclosed by a larger skyrmion bag of opposite polarity, giving a total skyrmion number of $|N_{sk}| = n - 1$ (see inset). Notably, the skyrmion bag topology was previously proposed in liquid crystals and magnetic systems[34], and more recently observed in surface plasmon polaritons on metal surfaces[15]. In contrast, the skyrmion bags demonstrated here are realised in freespace light fields that can propagate over arbitrarily long distances while preserving their topology.

II. RESULTS OF SUPERTOPOLOGIES

To show the proof of concept, we experimentally realise the freespace supertopologies using a spatial light modulator (SLM) (see Supplementary Material S1). We first present the results for twisted C_6-based skyrmionium lattices at $\theta = 13.2°$, where superlattices of skyrmionium bags act as supercells arranged in long-range C_6 symmetry. Figure 2(a1) shows the measured long-range order

in the out-of-plane Stokes vector S_z, where the arrows indicate the unit vectors defining the hexagonal supercells formed by the skyrmionium bags. The polarization texture of the central skyrmionium bag is shown in Fig. 2(a2), where the white dash–dot line marks the boundary of the skyrmionium cluster formed by seven individual skyrmioniums. This cluster is enclosed within a larger skyrmionium bag of opposite polarity, whose boundary is outlined by the dashed white curve. The boundaries are identified using a computational Snake algorithm (see Methods). Figure 2(a3) shows the measured skyrmion density for the central skyrmionium bag. As evident, the elementary skyrmioniums within the cluster share the same vorticity as the surrounding bag skyrmionium but with opposite polarity. The measured skyrmion numbers of the entire skyrmionium bag and its inner skyrmion cluster are both close to zero, whereas each baby skyrmion embedded in the cluster exhibits a near-unit topology ($N_{\mathrm{sk}} > 0.9$).

As the twist angle increases to $\theta = 16.4°$, the overall long range C_6 symmetry begins to break down. Figure 2(b1) shows that while the central skyrmionium bag remains intact, the surrounding region becomes aperiodic and no longer forms a regular superlattice. The corresponding polarization and skyrmion density maps (Figs. 2(b2,b3)) confirm that the core topology of the central skyrmionium bag is preserved despite the loss of long-range order, demonstrating its resilience against twist angle deviation. Further increasing the twist angle to $\theta = 21.8°$ leads to a topological transition into the skyrmion cluster superlattice, as shown in Fig. 2(c1). This topological texture can be named as *skyrmion-skyrmionium bag*, where the center is a skyrmionium. This is a novel topology of skyrmion bag not realized before in plasmonics before. In this configuration, the supercells adopt a petal-like arrangement consisting of multiple skyrmion clusters surrounding a central skyrmionium. The polarization and skyrmion number density plots (Figs. 2(c2,c3)) show that the central skyrmionium and its protected skyrmion exhibit higher structural fidelity compared to the six surrounding petals.

At $\theta = 27.8°$, a nested superlattices emerges, where the basic central structure is a multi-π nested target skyrmion surrounded with multiple skyrmionium tiling the whole space, with global transitional symmetry (Fig. 2(d1)). The first three nested skyrmion at the center with measured skyrmion numbers close to ± 1 were analyzed in Figs. 2(d2,d3)

Furthermore, we generate diverse moiré supertopologies by performing freespace twistronics on C_4-based skyrmion lattices, resulting in skyrmion cluster superlattices that contain different numbers of skyrmions per supercell at different twist angles. At $\theta = 10.35°$, the moiré superlattice supercell contains 25 skyrmions (Figs. 2(e1–e3)). When the twist angle is increased to $\theta = 12.66°$, the structure transforms into a 13-skyrmion supercell (Figs. 2(f1–f3)), which remains stable up to $\theta = 16.26°$ (Figs. 2(g1–g3)). Further increase to $\theta = 22.61°$ results in a 5-skyrmion supercell (Figs. 2(h1–h3)). Simulation results corresponding to Figs. 2 are presented in Extended data Fig E4. For the C_4-based skyrmion lattices, there is no one-to-one mapping between the vortices and Gaussians in the LCP and RCP components, leading to intensity nulls or electromagnetic dark spots within the lattice. When such lattices are twisted, these intensity nulls persist in the resulting moiré superlattices, which can introduce small inaccuracies in the measurement of total skyrmion number. To ensure accurate measurements, a small correction term δ is added to the LCP component. Furthermore, freespace twistronics is also performed on C_3-based meron lattices, yielding complex meron–antimeron cluster supertopologies (see Supplementary Material S3).

Moreover, it has been shown that due to periodicity in the stokes vector, the topological lattices can be decomposed in sub-lattices of lower topologies. For example, a C_6 skyrmionium lattice can be decomposed in three different C_6 skyrmion sub-lattices of different periodicity. Similarly, a C_4 skyrmion lattice can be decomposed in two C_4 meron sub-lattices [25]. Therefore, in addition to the supertopologies discussed above, we can also achieve skyrmion bags, skyrmion petal superlattices, lower-order topological quasicrystals, and so on. To observe freespace skyrmion bag superlattices, we need the optical lattice decomposition method[25]. Similar to the Stokes vector of individual C_6 skyrmionium lattices, the Stokes vector of twisted superlattice also exhibits periodicity, leading to various spatial frequency components. Therefore, by selective spatial decomposition, lower order topologies can be obtained. Figure 3(a1) shows the spatial Fourier spectrum of the Stokes vector (Fig. 2(b1)) corresponding to skyrmionium bag superlattice obtained by twisting two elementary skyrmionium lattices at an angle of $\theta = 16.4°$. The Fourier spectrum can be divided into seven sets of spatial frequency components (shown by white dashed circles in Fig. 3(a1)). Figures 3(a2-a8) show 7 real-space textures which are obtained from the seven different spatial frequency circles. These textures resemble with C_6 skyrmion lattices, as well as skyrmion bags in bilayer and trilayer moiré skyrmion superlattices. Spatial frequencies consisting of only six spots results in C_6 skyrmion lattices in real space with different lattice vectors (Figs. 3(a2-a8). However, sets of spatial frequencies consisting of more than six spots, i.e. k_1 and k_2 with twelve and k_3 with eighteen spots results in higher order super topologies. Note, k_1 and k_2 results in skyrmion bag corresponding consisting of seven elementary skyrmions (Fig. 3(a3)-(a6)) representing bilayer twisting of skyrmion lattices, whereas, k_3 generates a bigger skyrmion bag with eighteen elementary skyrmions (Fig. 3(a8)) which represents trilayer twisting of skyrmion lattices. Figure 3(b1) shows the experimental results of the skyrmion bag, where the $n = 7$ baby skyrmions are inside with measured $N_{\mathrm{sk}} = -6.83$ surrounded with a bag skyrmion of opposite polarity with $N_{\mathrm{sk}} = 0.81$, thus, the total skyrmion number is $N_{\mathrm{sk}} = -6.83 + 0.81 = -6.02$ and its absolute

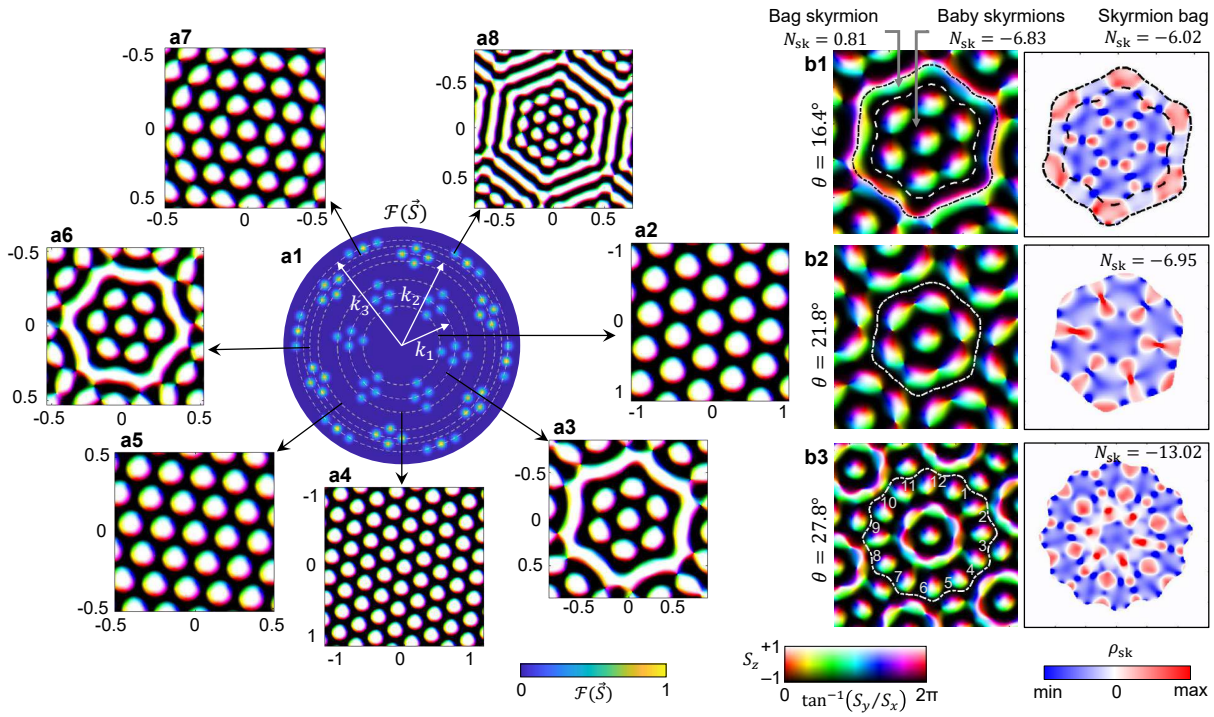

FIG. 3: **Hierarchical supertopology decomposition.** (a1) Theoretical spatial Fourier spectrum of stokes vector of a skyrmionium bag superlattice at $\theta = 16.4°$, where the distribution is located at a set of concentric circles in wavenumber-space, and (a2-a8) the corresponding hierarchical real-space textures as skyrmion lattices and skyrmion bag superlattices. The white arrows in (a1) mark the three circles of wavenumber radii k_1, k_2, and k_3 for the cases of skyrmion bag generation. (b1-b3) Experimental results of skyrmion bag, skyrmion cluster superlattices, and topological quasicrystal, with measured textures and skyrmion density distributions, at twisted angles of 16.4°, 21.8°, and 27.8°, respectively, measured skyrmion numbers of selected topological featured in dashed lines are marked. Unit of coordinates: mm.

value is close to the idea $n - 1 = 6$ (Fig. 3(b1)). If we do same decomposition to morié textures at $\theta = 21.8°$, we can obtain skyrmion cluster superlattice, where the supercell is petal like cluster of 7 skyrmions (Fig. 3(b2)). At $\theta = 27.8°$, the decomposed morié texture shows a lower-order topological nested superlattices, where the basic structure is a 3π target skyrmion surrounded with 12 skyrmions, thus the total skyrmion number is close to $|N_{sk}| = 13$ (Fig. 3(b3)) Complete hierarchical supertopology decomposition for other twist angles is shown in extended data Fig. E5. Furthermore, hierarchical supertopology decomposition for twisted C_4 skyrmion lattices and C_3 meron-antimeron lattices reveals sublattices of lower topologies such as meron-antimeron lattices and clusters (see Supplementary Material S2-S4). We can apply such decomposition to other morié supertopologies to access more kinds of topologies.

III. ROBUSTNESS UPON PROPAGATION

The supertopologies are generated by twisting the light fields of two elementary topological lattices. Therefore, they exhibit the propagation properties of elementary lattices. For example, light field of elementary C_6 skyrmionium lattice is composed of only one radial frequency component with six point sources. Therefore, the light field from six point sources diffracts equally and results in non-diffracting and propagation invariant behavior in the interference region. In contrast to conventional skyrmionic or bimeronic beams where they are divergent but topologically invariant upon propagation[35], here, the topological features and geometric shape and size the supertopologies all do not change at all. Figures 4(a,b) show experimentally measured skyrmion bag textures upon propagation through 50 cm, in twisted C_6 skyrmionium lattices at $\theta = 13.2°$ (superlattice case) and 16.4° (isolated case). In both cases, the geometric sizes and topological features are invariant, only with local helicity evolves with dynamic phase upon propagation, see details in Extended data figure E6-E7. Figures 4(a2,b2) are corresponding simulated and experimental skyrmion numbers for the skyrmionium bags ($n = 7$) and the protected baby skyrmions in which (the error bars evaluate the numerical difference for the 7 baby skyrmions). The results prove that the supertopology is resilient to both dynamic propagation and twisted angle deviations.

Figures 4(c,d) show experimentally measured non-diffractive propagation-dependent geometry-independent skyrmion clusters, in twisted C_4 skyrmion lattices at $\theta = 10.35°$ and 12.7° for $n = 25$ and $n = 13$, respec-

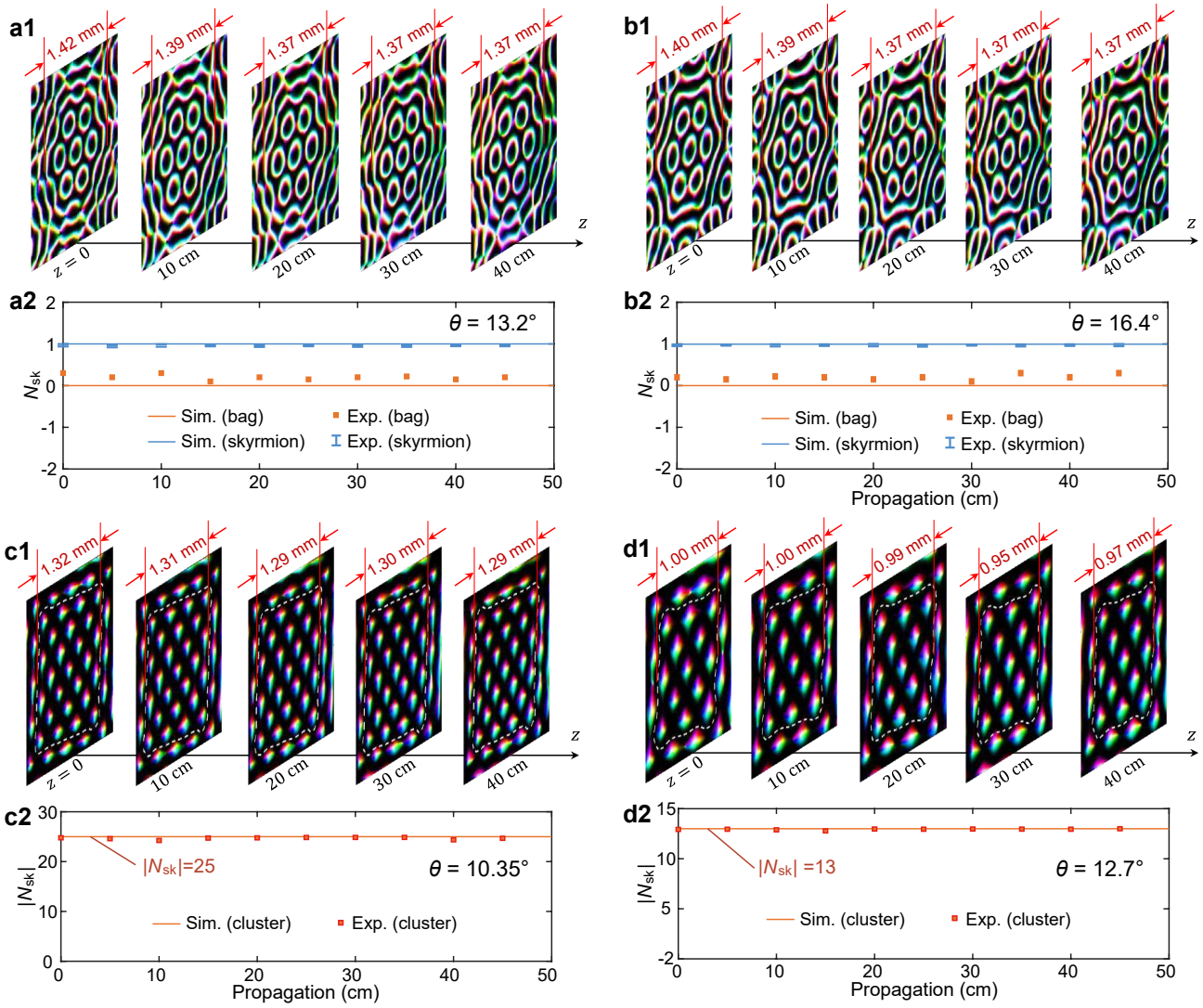

FIG. 4: **Nondiffracting topologically stable propagation.** (a1-d1) Experimental results of the propagation-dependent supertopological textures for two skyrmionium bags at $\theta = 13.2°$ and 16.4° and two skyrmion clusters at $\theta = 10.35°$ and 12.7°, respectively, form $z = 0$ to 50 cm. The featured side is marked correspondingly in each texture pattern. (a2,b2) The simulated and experimental skyrmion numbers for the skyrmionium bags ($n = 7$) and the protected baby skyrmions in which (the error bars evaluate the numerical difference for the 7 baby skyrmions), corresponding to (a1,b1). (c2,d2) The simulated and experimental skyrmion numbers for the skyrmion clusters ($n = 25$ and $n = 13$), corresponding to (c1,d1).

tively. The measured skyrmion numbers agree very well with the theoretical prediction, see Figs 4(c1,d1). Please see details in Extended data figure E6-E7.

Hereinafter, we show the nondiffractive supertopologies are even strongly resilient to obstacles. Notably, the topological protection of skyrmions were previously studied[36,37], however, which are only for complex transparent and scattering media, and no similar studies to topological lattices is proposed. The blocking of solid obstacles are of stronger perturbation in contrast to complex media, the optical mode revival after obstacles in propagation path is usually called self-healing effect[38], the topology self-healing of skyrmionic beam was also studied recently[39], but again, not for topological lattice.

Figures 5(a,b) show our experimental results of skyrmionium bag propagation passing through obstacles of consisting of one disk (a) and two disks (b), blocking one and two skyrmioniums in the bag, respectively. The simulated and experimental skyrmion number versus propagation for the baby skyrmion protected in the blocked skyrmionium and that two in the two blocked skyrmioniums ("α" and "β") are shown in Fig. 5(c-e), respectively. Please see simulation results in Extended data figure E8.

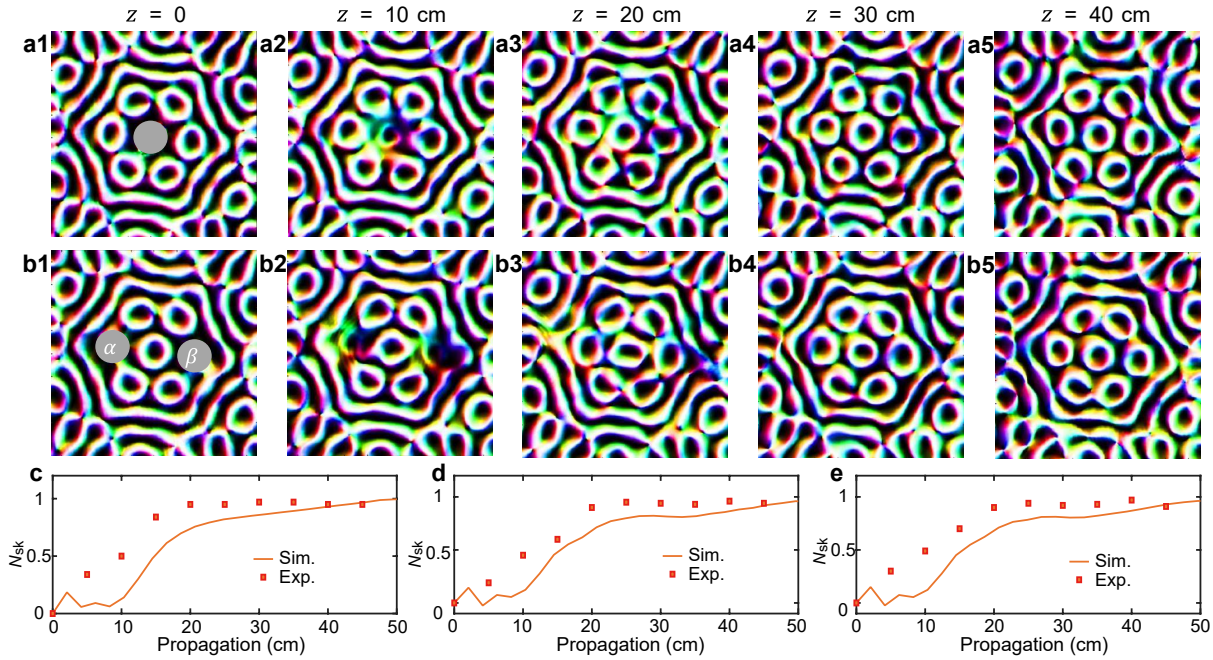

FIG. 5: **Self-healing topologies against obstacles.** Experimental results of skyrmionium bag propagation passing through obstacles for (a1) a disk, marked in gray, blocking the center skyrmionium and (a2) two disks blocking two skyrmioniums in bag, at $z = 0$. (c-e) The simulated and experimental skyrmion number versus propagation for the baby skyrmion protected in the blocked skyrmionium in (a1) and that two in the two blocked skyrmioniums ("α" and "β") in (b1), respectively.

IV. DISCUSSION

We proposed the concept of freespace twistronics and successfully demonstrated emerging supertopologies controlled in the twisted morié structured light, opening many exciting possibilities of new directions. Many novel topologies, skyrmionium bags, skyrmion-bag superlattices, supertopological quasicrystals, etc., not accessible in any physical system before, now, can be simply generated in twisted bi-volume morié structured light. In this work, we only considered superposition of two layers. It can be extended to morié-of-morié scheme as recently emerging trilayer lattices[3,40] and twisted multilayer[6] for opening unlimited exploration of more nontrivial topologies.

Breaking 2D limit of prior twistronics, we open new dimensions and more degrees of freedom for 3D even 4D space-time twistronics. In this work, we only considered coaxial twisting, while, for emerging 3D freespace topological optical field, e.g. the space-time hopfion crystals[27], we can open 3D twisting of multiple topological along arbitrary axial orientations for potential higher-dimensional space-time supercrystals.

Here, we focus on exploring topological textures of light. More properties of structured light can be studied in the framework of freespace twistronics, such as energy localization[11] and superoscillation[41].

In contrast to any prior model of morié electronics and photonics relying on responses of materials, our freespace morié supertopological light can propagate so as to interact with matter, potentially transfer optical topologies to matter, as a new methodology to excite physical effects, atomic topologies[42], for atom trapping[43,44], structured light directly writing topological solitons of matter.

Optical supertopologies are highly ondemand for next-generation information carriers to revolutionize our optical communication network[45]. As their diversified control of topological textures, higher capacity data encoding and transfer can be promised, meanwhile, the enhanced robustness can be expected due to the nondiffraction and resilience of supertopologies. We plan to apply supertopologies for communication and encryption, overcoming the bottleneck of current optical vortex techniques.

Supertopologies were firstly generated in light waves here, which will certainly motivate the exploration of supertopologies in other waves, e.g. sound waves and water waves, as well as the exploration of supertopologies in matter, i.e. liquid crystals, chiral magnets and beyond.

Data availability

The data that support the findings of this study are available within the paper and the Extended Data. Other relevant data are available from the corresponding authors on reasonable request.

Acknowledgements

Authors thank Julian Schwab for useful discussions. Authors thank Singapore Ministry of Education (MOE) AcRF Tier 1 grants (RG157/23 & RT11/23), Singapore Agency for Science, Technology and Research (A*STAR)

MTC Individual Research Grants (M24N7c0080), and Nanyang Assistant Professorship Start Up grant.

Author Contributions

Y. S. conceived the idea and supervised the project; V. D. developed the theoretical simulation and experiments; All authors analyzed the data and prepared the manuscript.

Conflict of Interest

The authors declare no conflict of interest.

* Electronic address: yijie.shen@ntu.edu.sg

[1] Carr, S. *et al.* Twistronics: Manipulating the electronic properties of two-dimensional layered structures through their twist angle. *Physical Review B* **95**, 075420 (2017).

[2] Cao, Y. *et al.* Unconventional superconductivity in magic-angle graphene superlattices. *Nature* **556**, 43–50 (2018).

[3] Park, J. M., Cao, Y., Watanabe, K., Taniguchi, T. & Jarillo-Herrero, P. Tunable strongly coupled superconductivity in magic-angle twisted trilayer graphene. *Nature* **590**, 249–255 (2021).

[4] Cao, Y. *et al.* Correlated insulator behaviour at half-filling in magic-angle graphene superlattices. *Nature* **556**, 80–84 (2018).

[5] Cao, Y. *et al.* Tunable correlated states and spin-polarized phases in twisted bilayer–bilayer graphene. *Nature* **583**, 215–220 (2020).

[6] Törmä, P., Peotta, S. & Bernevig, B. A. Superconductivity, superfluidity and quantum geometry in twisted multilayer systems. *Nature Reviews Physics* **4**, 528–542 (2022).

[7] Du, L. *et al.* Moiré photonics and optoelectronics. *Science* **379**, eadg0014 (2023).

[8] Ciarrocchi, A., Tagarelli, F., Avsar, A. & Kis, A. Excitonic devices with van der waals heterostructures: valleytronics meets twistronics. *Nature Reviews Materials* **7**, 449–464 (2022).

[9] Hu, G. *et al.* Topological polaritons and photonic magic angles in twisted α-moo3 bilayers. *Nature* **582**, 209–213 (2020).

[10] Ji, Z. *et al.* Opto-twistronic hall effect in a three-dimensional spiral lattice. *Nature* **634**, 69–73 (2024).

[11] Wang, P. *et al.* Localization and delocalization of light in photonic moiré lattices. *Nature* **577**, 42–46 (2020).

[12] Luan, H.-Y., Ouyang, Y.-H., Zhao, Z.-W., Mao, W.-Z. & Ma, R.-M. Reconfigurable moiré nanolaser arrays with phase synchronization. *Nature* **624**, 282–288 (2023).

[13] Ouyang, Y.-H., Luan, H.-Y., Zhao, Z.-W., Mao, W.-Z. & Ma, R.-M. Singular dielectric nanolaser with atomic-scale field localization. *Nature* **632**, 287–293 (2024).

[14] Xu, G. *et al.* Hydrodynamic moiré superlattice. *Science* **386**, 1377–1383 (2024).

[15] Schwab, J. *et al.* Skyrmion bags of light in plasmonic moiré superlattices. *Nature Physics* 1–7 (2025).

[16] Jani, H. *et al.* Antiferromagnetic half-skyrmions and bimerons at room temperature. *Nature* **590**, 74–79 (2021).

[17] Tang, J. *et al.* Magnetic skyrmion bundles and their current-driven dynamics. *Nature Nanotechnology* **16**, 1086–1091 (2021).

[18] Zheng, F. *et al.* Hopfion rings in a cubic chiral magnet. *Nature* **623**, 718–723 (2023).

[19] Wu, J.-S. & Smalyukh, I. I. Hopfions, heliknotons, skyrmions, torons and both abelian and nonabelian vortices in chiral liquid crystals. *Liquid Crystals Reviews* **10**, 34–68 (2022).

[20] Wu, H. *et al.* Photonic torons with 3d topology transitions and tunable spin monopoles. *Physical Review Letters* **135**, 063802 (2025).

[21] Tsesses, S. *et al.* Optical skyrmion lattice in evanescent electromagnetic fields. *Science* **361**, 993–996 (2018).

[22] Lei, X. *et al.* Photonic spin lattices: symmetry constraints for skyrmion and meron topologies. *Physical Review Letters* **127**, 237403 (2021).

[23] Marco, D., Herrera, I., Brasselet, S. & Alonso, M. A. Periodic skyrmionic textures via conformal cartographic projections. *APL Photonics* **9** (2024).

[24] Marco, D., Herrera, I., Brasselet, S. & Alonso, M. A. Propagation-invariant optical meron lattices. *ACS Photonics* **11**, 2397–2405 (2024).

[25] Teng, H., Zhong, J., Lei, X. & Zhan, Q. Topological decomposition of hierarchical skyrmion lattices. *Communications Physics* **8**, 99 (2025).

[26] Wu, H., Zhou, W., Zhu, Z. & Shen, Y. Optical skyrmion lattices accelerating in a free-space mode. *APL Photonics* **10** (2025).

[27] Lin, W., Mata-Cervera, N., Ota, Y., Shen, Y. & Iwamoto, S. Space-time optical hopfion crystals. *Physical Review Letters* **135**, 083801 (2025).

[28] Shen, Y. *et al.* Optical skyrmions and other topological quasiparticles of light. *Nature Photonics* **18**, 15–25 (2024).

[29] Bogdanov, A. N. & Panagopoulos, C. Physical foundations and basic properties of magnetic skyrmions. *Nature Reviews Physics* **2**, 492–498 (2020).

[30] Shen, Y., Wang, H. & Fan, S. Free-space topological optical textures: tutorial. *Advances in Optics and Photonics* **17**, 295–374 (2025).

[31] Tsesses, S. *et al.* Four-dimensional conserved topological charge vectors in plasmonic quasicrystals. *Science* **387**, 644–648 (2025).

[32] Putley, H. J., Davies, B., Rodríguez-Fortuño, F. J., Bykov, A. Y. & Zayats, A. V. Mixing skyrmions and merons in topological quasicrystals of the evanescent optical field. *Optica* **12**, 614–619 (2025).

[33] Lin, M. *et al.* Photonic quasicrystal of spin angular momentum. *Science Advances* **11**, eadv3938 (2025).

[34] Foster, D. *et al.* Two-dimensional skyrmion bags in liquid crystals and ferromagnets. *Nature Physics* **15**, 655–659 (2019).

[35] Shen, Y. Topological bimeronic beams. *Optics Letters* **46**, 3737–3740 (2021).

[36] Wang, A. A. *et al.* Topological protection of optical skyrmions through complex media. *Light: Science & Applications* **13**, 314 (2024).

[37] Zhang, Z. *et al.* Topological protection degrees of optical skyrmions and their electrical control. *Photonics Research* **13**, B1–B11 (2025).

[38] Shen, Y., Pidishety, S., Nape, I. & Dudley, A. Self-healing of structured light: a review. *Journal of Optics* **24**, 103001

(2022).
[39] Guo, H. *et al.* Self-healing of optical skyrmionic beams. *Journal of Optics* **27**, 025604 (2025).
[40] Park, D. *et al.* Unconventional domain tessellations in moiré-of-moiré lattices. *Nature* 1–8 (2025).
[41] Ma, X. *et al.* Observation of superoscillation superlattices. *arXiv preprint arXiv:2409.19565* (2024).
[42] Mitra, C. *et al.* Topological optical skyrmion transfer to matter. *APL Photonics* **10** (2025).
[43] Yu, J.-C., Bhave, S., Reeve, L., Song, B. & Schneider, U. Observing the two-dimensional bose glass in an optical quasicrystal. *Nature* **633**, 338–343 (2024).
[44] Meng, Z. *et al.* Atomic bose–einstein condensate in twisted-bilayer optical lattices. *Nature* **615**, 231–236 (2023).
[45] Wan, Z., Wang, H., Liu, Q., Fu, X. & Shen, Y. Ultra-degree-of-freedom structured light for ultracapacity information carriers. *ACS Photonics* **10**, 2149–2164 (2023).
[46] Kass, M., Witkin, A. & Terzopoulos, D. Snakes: Active contour models. *International journal of computer vision* **1**, 321–331 (1988).

V. METHODS

Characterization of skyrmion and its boundary The topological properties of the optical quantum skyrmions can be characterized by the skyrmion number, which is defined as[28]

$$N_{\mathrm{sk}} = \frac{1}{4\pi} \iint_{\sigma} \boldsymbol{n} \cdot \left(\frac{\partial \boldsymbol{n}}{\partial x} \times \frac{\partial \boldsymbol{n}}{\partial y} \right) dxdy \ ,$$

where $\boldsymbol{n}(x, y)$ represents the Stokes vectors to construct a skyrmion and σ denotes the skyrmion area. For the experimentally measured Stokes fields, we applied linear interpolation followed by a Gaussian filter as part of the post-processing procedure to suppress noise and enhance the accuracy of the skyrmion number calculation. Besides, due to the different size of the skyrmionic Stokes fields, careful area selection was crucial.

Ideally, the Stokes skyrmion is well-defined with clear circular symmetry, allowing the topological charge to be determined by integrating over a circular contour. However, turbulence disrupts this symmetry and a circular integral no longer gives us the correct topological charge. Therefore, it is necessary to accurately define an adaptive contour that accurately captures the topological charge. Here, we applied the Active Contour Model (ACM), otherwise known as Snakes[46]. Snakes are an unparalleled tool widely employed in computer vision, primarily used to outline an object's boundary in a noisy two-dimensional environment. They are adaptive, energy-minimizing contours that evolve iteratively under the influence of internal and external forces, denoted by E_{int} and E_{ext}, respectively. Mathematically, the Snake's energy function is given by:

$$E_{\mathrm{snake}} = \int_0^1 (E_{\mathrm{int}} + E_{\mathrm{ext}})\, ds \ ,$$

where ds represents the differential element of the curve parameter. The optimization of the snake function is based on the concept of gradient descent. Starting from an initial contour, the algorithm iteratively minimizes the Snake function's energy, moving in the direction of the negative gradient at each step. This process continues until the local minima are found, at which point the contour outlines the boundary of the image.

EXTENDED DATA

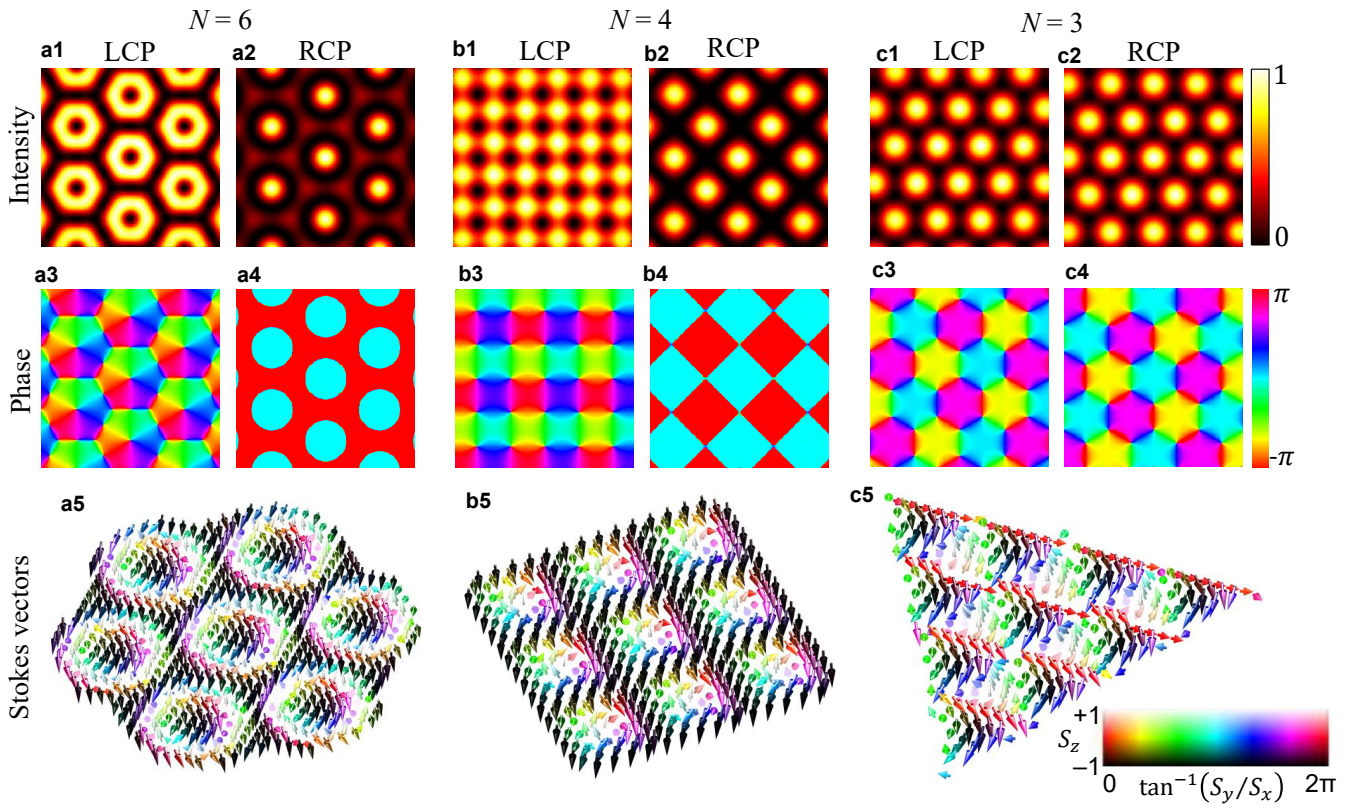

FIG. E1: **Basic topological lattices.** (a1-a2) Intensity and (a3-a4) phase distribution of LCP and RCP whereas, (a5) stokes vector topological texture for C_6 skyrmionium lattices. (b1-b2) Intensity and (b3-b4) phase distribution of LCP and RCP whereas, (b5) stokes vector topological texture for C_4 skyrmion lattices. (c1-c2) Intensity and (c3-c4) phase distribution of LCP and RCP whereas, (c5) stokes vector topological texture for C_3 meron-antimeron lattices.

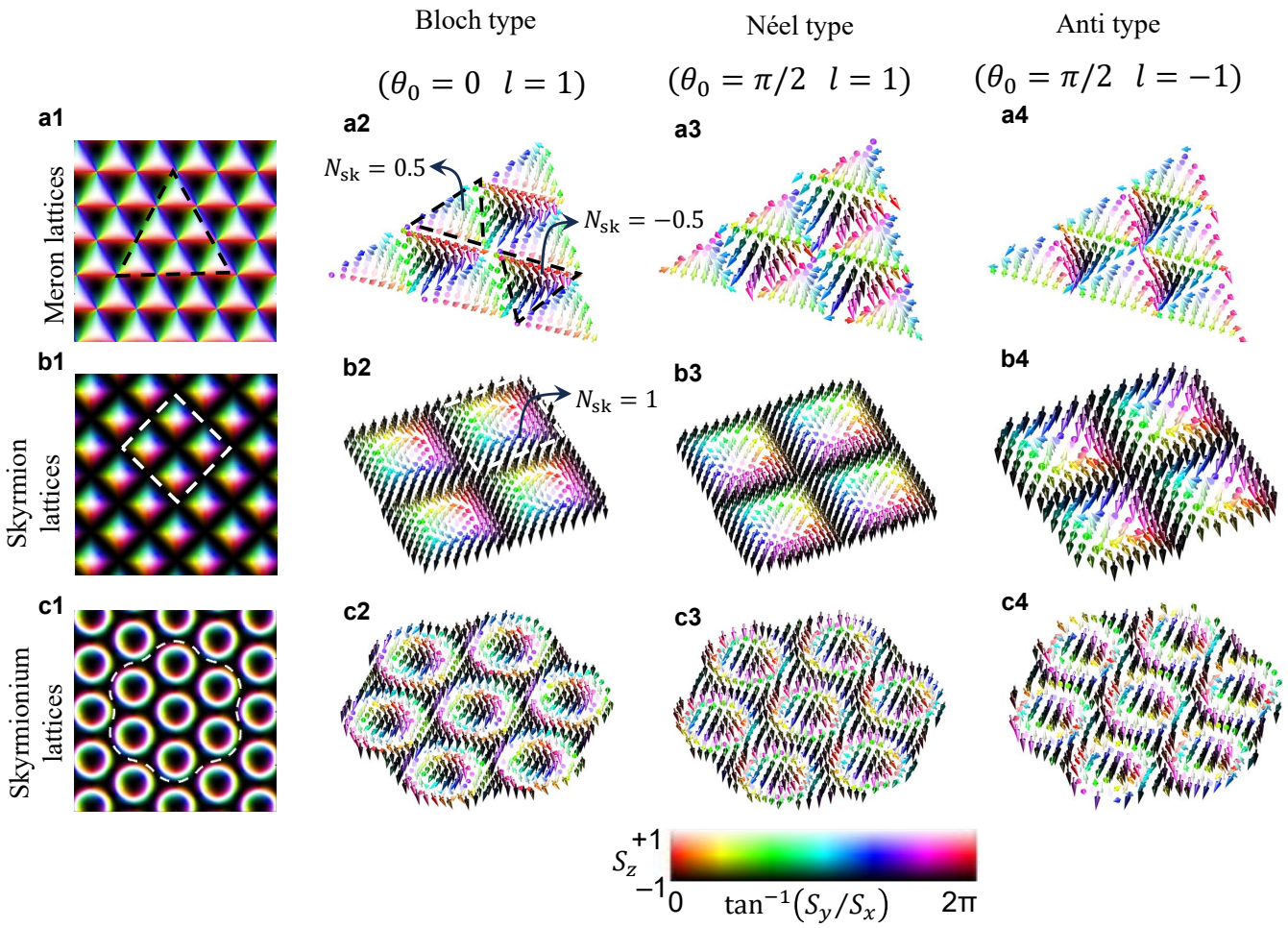

FIG. E2: **Diverse topological lattices.** (a1-a4) Skyrmion texture and stokes vectors for Bloch, Nèel and anti type C_3 meron-anti meron lattices. (b1-b4) Skyrmion texture and stokes vectors for Bloch, Nèel and anti type C_4 skyrmion lattices. (c1-c4) Skyrmion texture and stokes vectors for Bloch, Nèel and anti type C_6 skyrmionium lattices.

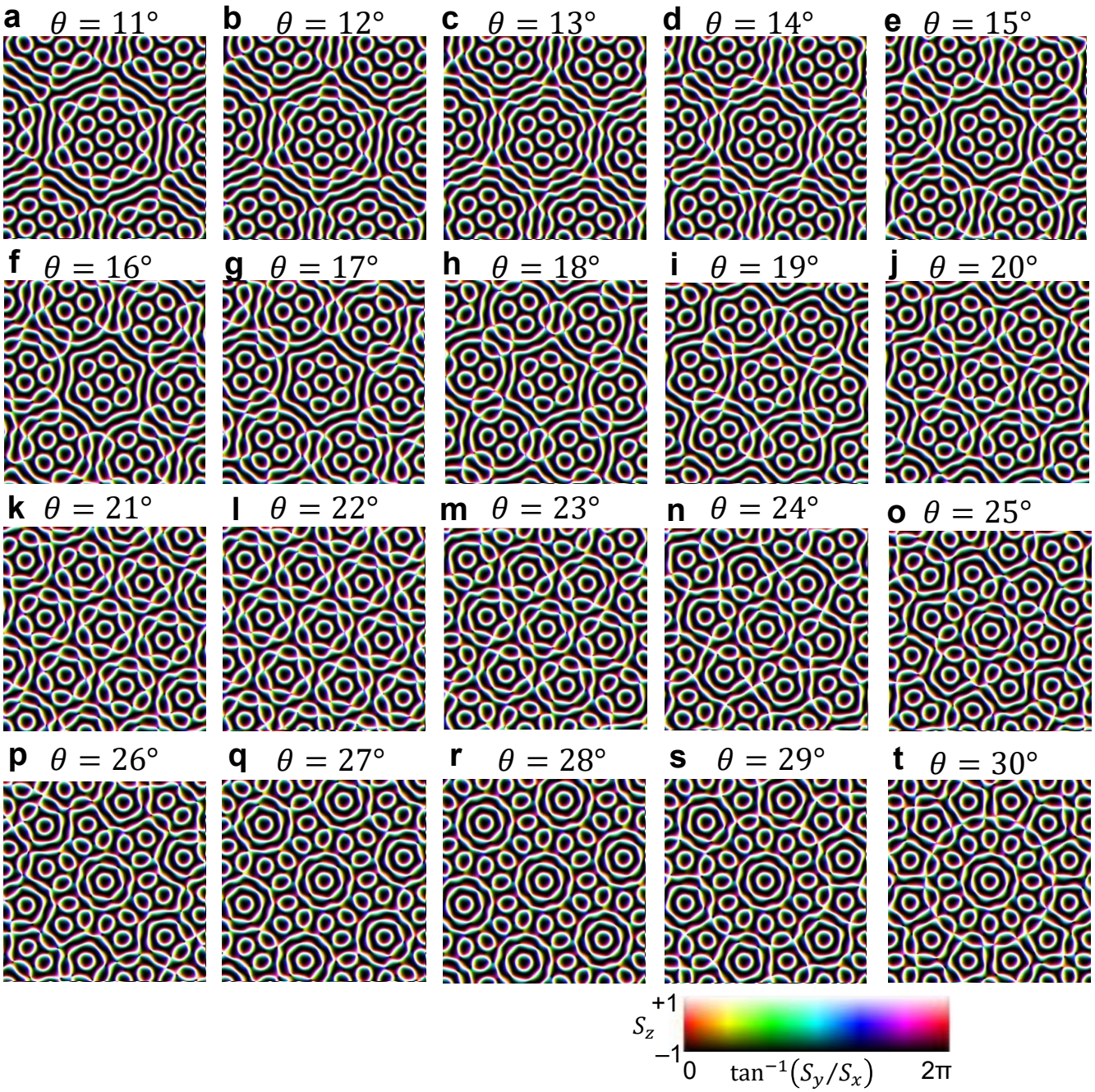

FIG. E3: **Different supertopologies for various twist angles.** (a-t) skyrmion texture for supertopologies obtained for twist angles $\theta = 11^\circ - 30^\circ$ for C_6 skyrmionium lattices.

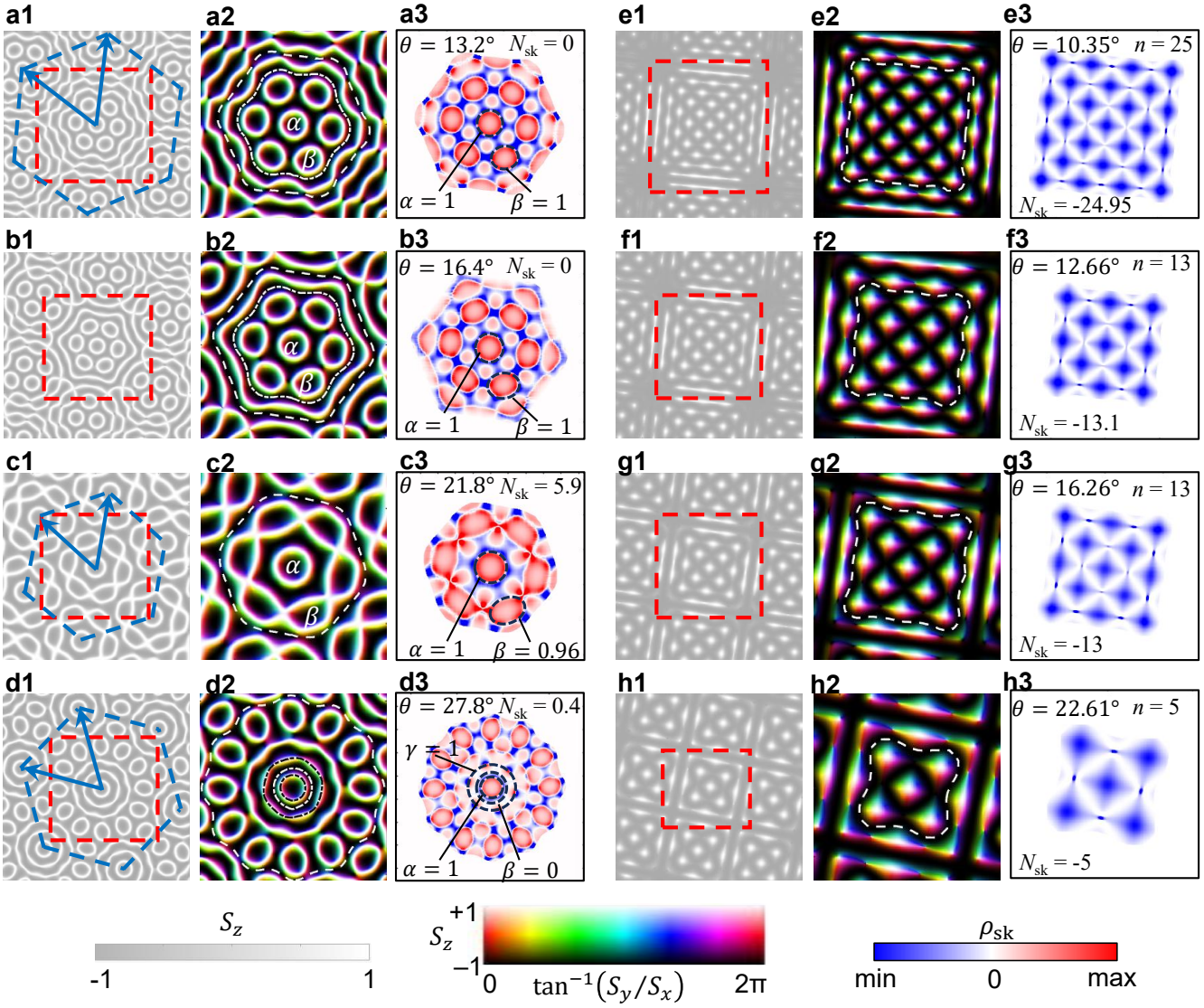

FIG. E4: **Simulation results for various supertopologies.** Long-range distributions of S_z, spin textures of featured topological structures (in red-dashed line boxes of long-range patterns correspondingly), and corresponding skyrmion density distributions for twisted C_6 skyrmionium lattices obtaining (a1-a3) skyrmionium bag superlattices at $\theta = 13.2°$ (blue arrows mark the long-range periodic unit vectors of supercell), (b1-b3) isolated skyrmionium bag at $\theta = 16.4°$, (c1-c3) skyrmion cluster superlattices at $\theta = 21.8°$, (d1-d3) nested superlattice at $\theta = 27.8°$; and for twisted C_4 skyrmion lattices obtaining skyrmion cluster superlattices for different baby skyrmion numbers in supercell of (e1-e3) $n = 25$ at $\theta = 10.35°$, (f1-f3) $n = 13$ at $\theta = 12.66°$, (g1-g3) $n = 13$ at $\theta = 16.26°$, (h1-h3) $n = 5$ at $\theta = 22.61°$. The experimental skyrmion numbers N_{sk} of featured supertopologies, marked by big dashed lines in (a2-h2), are shown in (a3-h3), respectively. The experimental N_{sk} values of selected protected baby skyrmions ("α","β","γ",) marked by black dashed lines are shown in (a3-d3), correspondingly.

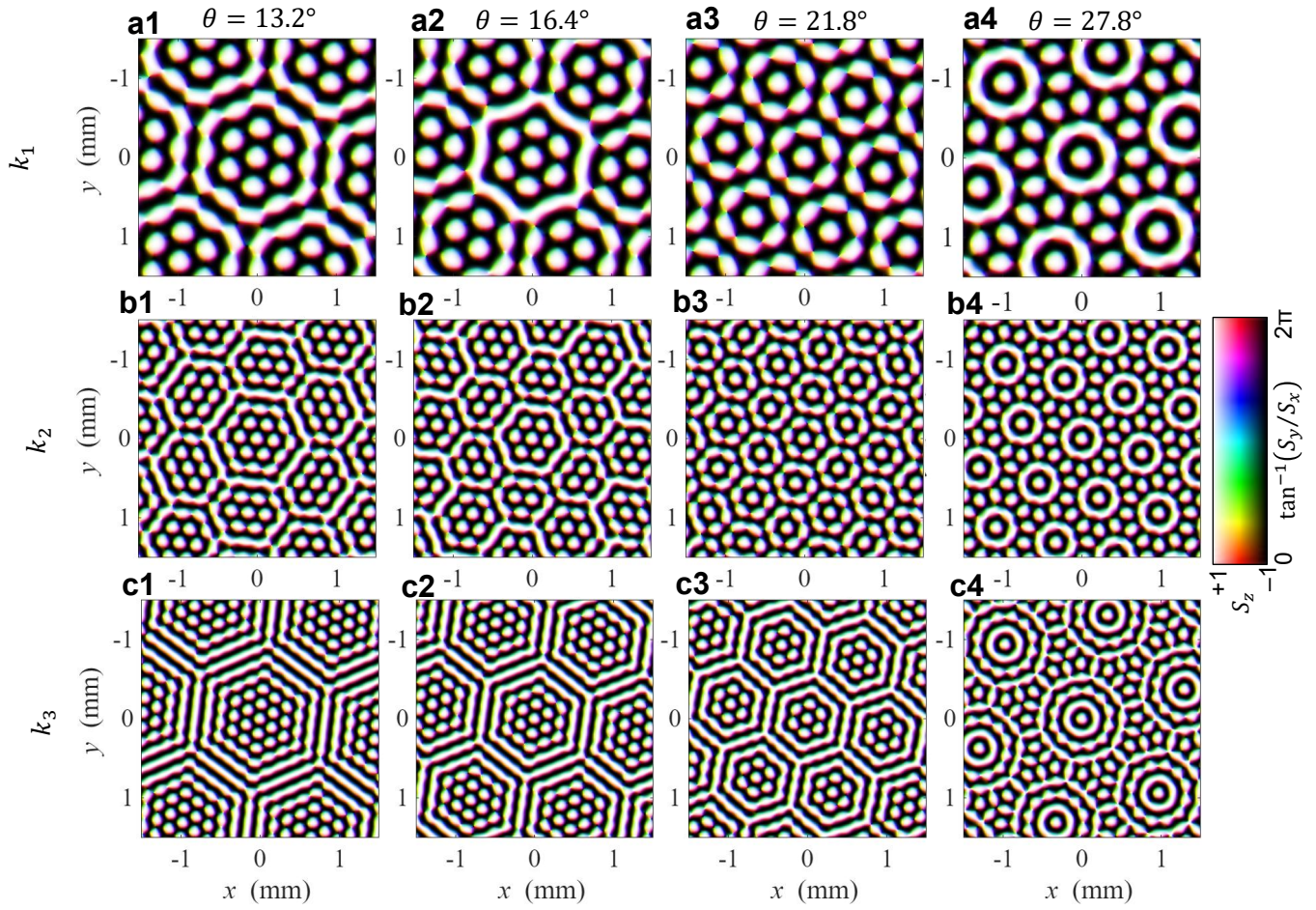

FIG. E5: **Hierarchical supertopology decomposition.** Decomposed skyrmion supertopologies generated from wavevectors (a1-a4)k_1, (b1-b4) k_2 and (c1-c4) k_3 obtained from the Fourier transform of stokes vectors of C_6 skyrmionium lattices twisted at $\theta = 13.2^\circ,\ 16.4^\circ,\ 21.8^\circ$, and 27.8°, respectively.

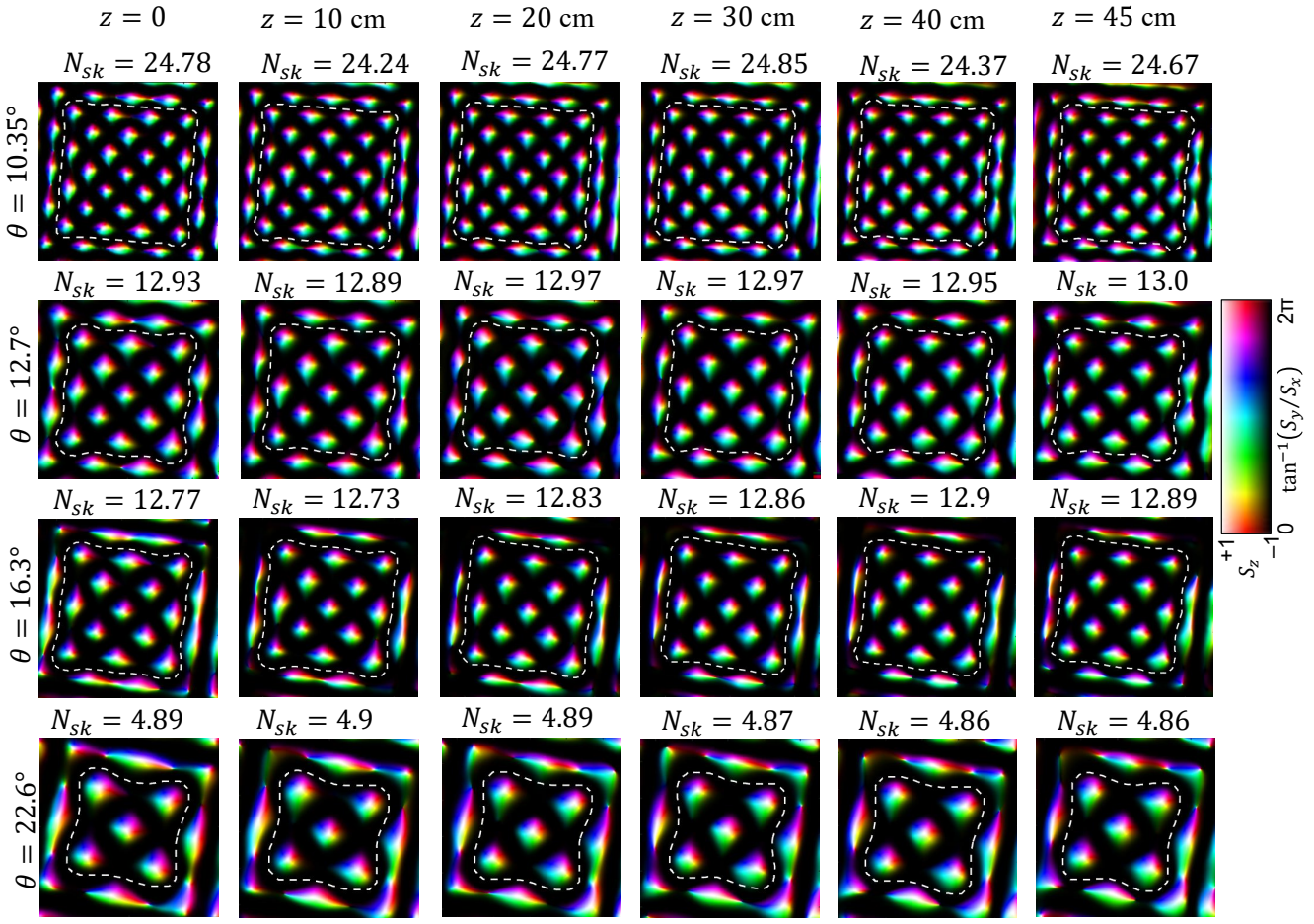

FIG. E6: **Experimental results for stable propagation of C_4 skyrmion cluster super lattices.** Stable propagation of skyrmion cluster superlattices obtained at twist angles $\theta = 10.35°$ (first row), $\theta = 12.7°$ (second row), $\theta = 16.3°$ (third row), and $\theta = 22.6°$ (fourth row).

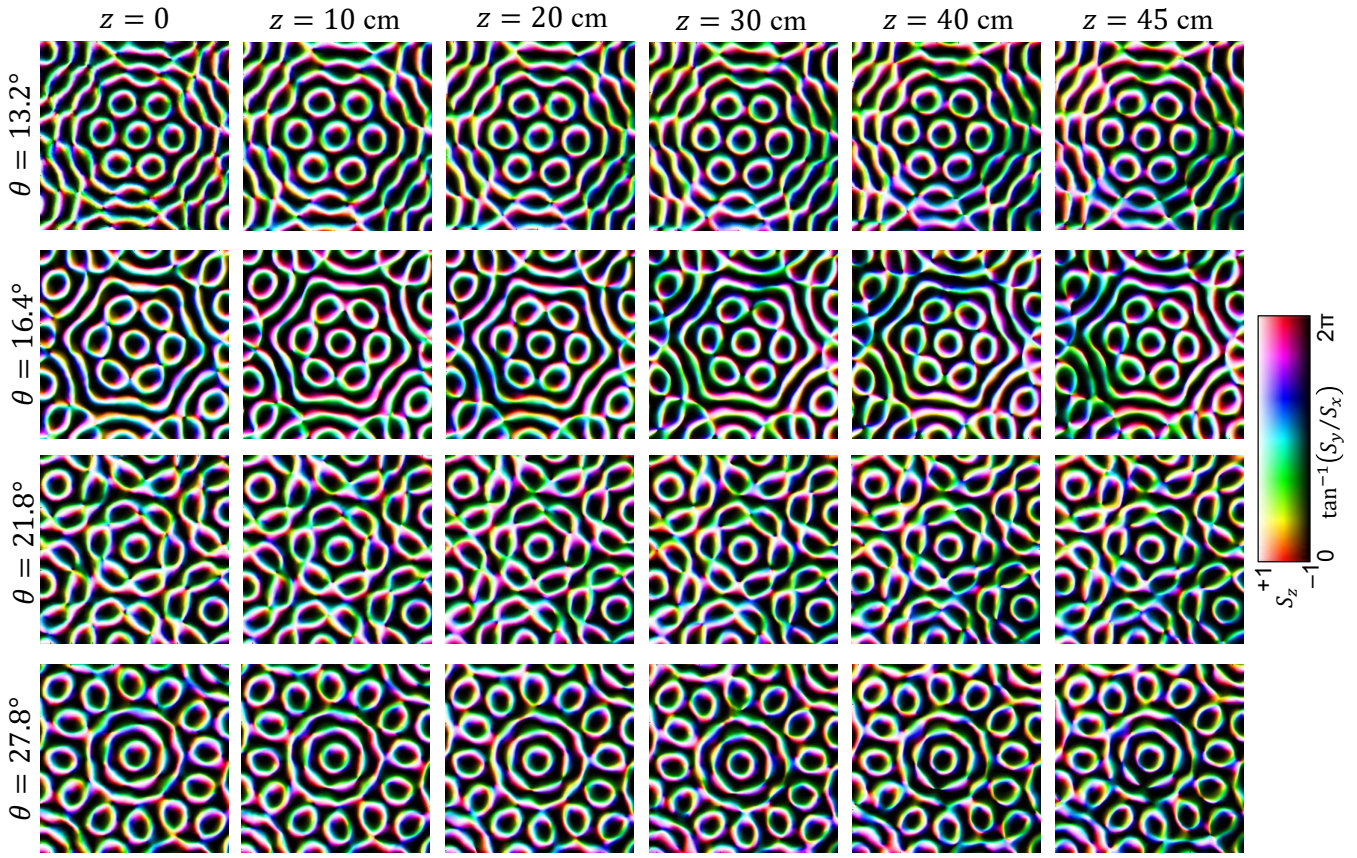

FIG. E7: **Experimental results for stable propagation of C_6 super topologies.** Stable propagation of skyrmionium super topologies obtained by twisting two skyrmionium lattices at twist angles $\theta = 13.2°$ (first row), $\theta = 16.4°$ (second row), $\theta = 21.8°$ (third row), and $\theta = 27.8°$ (fourth row).

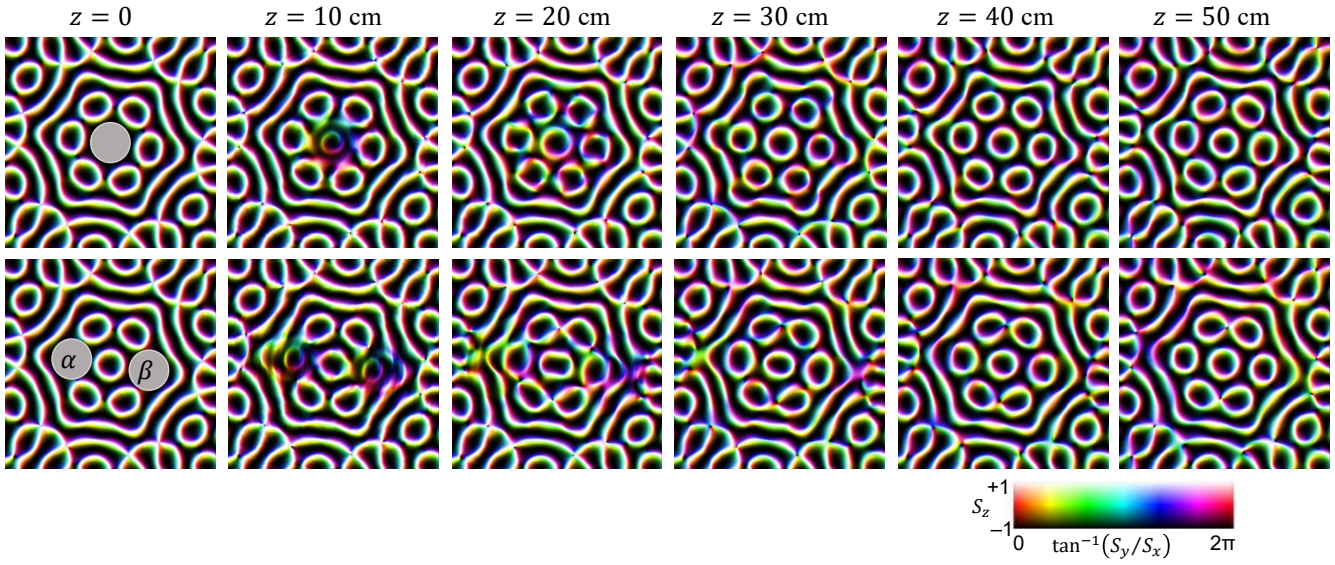

FIG. E8: **Simulation results for self-healing.** Self-healing of skyrmionium bag when central skyrmionium (first row) and two distinct skyrmioniums marked as α and β (second row) are blocked at $z = 0$.

Supplementary Files

This is a list of supplementary files associated with this preprint. Click to download.

- SM.pdf